Screening in Solutions of Star-Branched Polyelectrolytes

J. Klein Wolterink,[†] F. A. M. Leermakers,[†] G. J. Fleer,[†] L. K. Koopal,[†] E. B. Zhulina,[‡,§] and O. V. Borisov*[,†,§]

Laboratory for Physical Chemistry and Colloid Science, Wageningen Agricultural University, 6703 HB Wageningen, The Netherlands, Department of Chemical Engineering, University of Pittsburgh, Pittsburgh, Pennsylvania 15261, and Institute of Macromolecular Compounds, Russian Academy of Sciences, 199004 St. Petersburg, Russia

Received September 22, 1998; Revised Manuscript Received January 14, 1999

ABSTRACT: Equilibrium conformations of star-branched polyelectrolytes in dilute solutions are studied on the basis of a numerical self-consistent-field (SCF) approach and analytical theories. It is shown that, even in a dilute salt-free solution, the intramolecular Coulombic repulsion in many-armed stars is strongly screened by counterions which are localized preferentially in the intrastar space. As a result, the dependence of the star size on the number of branches levels off for many-armed stars. Addition of salt results in additional screening and in contraction of the stars. The scaling prediction $R \sim c_s^{-1/5}$ for the star size as a function of the salt concentration c_s is well confirmed by SCF calculations. A decrease in the star size can also be induced by an increase in the concentration of the polyelectrolyte in the solution. We have observed significant contraction of the stars with increasing concentration below the overlap threshold, i.e. in dilute solutions. The latter effect is more pronounced for stars with a small number of branches. The screening of the intramolecular Coulombic repulsion due to added salt is compared with that occurring upon increasing the concentration of the polyelectrolyte.

1. Introduction

Even though the properties of solutions of linear-chain polyelectrolytes are not completely understood,[1,2] charged polymers of more complex architecture, such as randomly or regularly branched polyelectrolytes or polyelectrolyte gels, attract strong attention.

Partially this is because of their relevance for practical applications, such as colloid stabilization.[3] Polyelectrolyte stars can be considered as models of micelles formed by hydrophobically modified polyelectrolytes in aqueous solutions[4−6] and for more complex practical systems like humic acids.

The behavior of charged polymers in the solution is determined by the interplay of long-range Coulombic interactions and effects of chain connectivity. From a theoretical point of view, the most important feature that makes polyelectrolyte solutions differ from those of ordinary low-molecular-weight electrolytes is essentially the nonlinear character of the screening of the Coulombic interactions. In other words, the linear Debye−Hückel (DH) approximation fails to describe the equilibrium properties of polyelectrolyte solutions, especially at low polyelectrolyte concentration and at low ionic strength of the solution.

The importance of nonlinear screening effects in polyelectrolyte solutions was understood early. The Manning counterion condensation concept[7] is the first example in this direction. We note that this type of condensation occurs only for strongly charged and stiff chains which retain local cylindrical symmetry on a large scale, exceeding the electrostatic screening length. In addition, nonlinear screening effects are also important for flexible polyelectrolytes in dilute solutions, even when they are only weakly charged. (In this paper, we discuss only quenched polyelectrolytes; the term "weak" refers to a small fraction of charged monomers.)

Several approaches[8−11] have been used to describe screening in dilute and semidilute solutions of weakly charged linear polyelectrolytes. They all are based on certain heuristic ideas which cannot be proved rigorously. Most of these theories[9−11] predict that screening of intra- and interchain Coulombic interactions in dilute polyelectrolyte solutions is stronger than follows from the linear DH approximation. Clearly, the most important question is what happens in the dilute solution. When the crossover concentration is defined, the properties in the semidilute regime can then be obtained from scaling arguments.

The essential feature of dilute solutions is the inhomogeneous distribution of counterions. Counterions are preferentially localized in the proximity of the polyions. The inhomogeneous distribution of counterions is also confirmed by simulations.[12] Therefore, for weakly charged linear chains, a scaling analysis that can deal only with power law dependencies is hardly feasible, even when the chains are very long.

The origin of the inhomogeneous distribution of counterions in dilute solutions is, of course, the strong Coulombic attraction between the counterions and the polyion, which carries a large net charge. The equilibrium distribution is determined by the competition between this attraction and the translational entropy of the counterions.

One can expect that this inhomogeneity is even stronger for branched polyions, where a comparatively large charge is immobilized in a small volume. This charge concentration must result in stronger attraction and less freedom for the counterions than in a solution of linear polyelectrolytes.

For strongly branched polyelectrolytes, the effect of the localization of counterions in the intramolecular volume appears to be strong enough to be treated on

* To whom correspondence should be addressed at BASF AG, ZX/ZC, Bau-13, D-67056 Ludwigshafen, Germany.
[†] Wageningen Agricultural University.
[‡] University of Pittsburgh.
[§] Rissian Academy of Sciences.

10.1021/ma981501w CCC: $18.00
Published on Web 03/12/1999

the level of a scaling approximation.[13−15] It was shown that, even in a very dilute solution, the high concentration of counterions inside the branched polyelectrolyte provides strong screening of Coulombic repulsion between charged monomers.

There are two important consequences from this trapping of counterions by strongly branched polyelectrolytes. First, the conformations of branched chains are less sensitive to the addition of salt because intramolecular repulsion is already screened. An increase in the salt concentration leads to additional screening and contraction of the branched polyelectrolyte only when this concentration exceeds the intrinsic concentration of counterions in the intramolecular space. Second, the effect of an increasing polymer concentration (in the dilute range) is expected to be weak in comparison to that in linear or weakly branched polyelectrolytes. This is because branched polyions release only a small fraction of their counterions into the intermolecular space. Hence, in a wide range, the intramolecular concentration of counterions (and the intramolecular screening) depends only weakly on the overall polyelectrolyte concentration.

Up to now, these effects in branched polyelectrolytes have been considered only on the basis of the scaling approximation.[13,14] From these predictions, the main power law dependencies for the structural properties of branched polyions are known. But this approximation cannot account for weaker non-power dependencies. The latter are expected to be rather important especially when the number of charges per branch is relatively low.

The aim of the present paper is to go beyond the scaling approximation and to analyze the screening effects in branched polyelectrolytes in dilute solution on the basis of a self-consistent-field (SCF) numerical approach, which on the mean-field level gives exact results, in combination with a strongly simplified analytical mean-field model. The results of the SCF calculations are compared to earlier scaling predictions, which serve as a guideline for a more elaborated analysis. We show that scaling gives a qualitatively correct description of the main trends in the behavior of branched polyelectrolytes in solution. For our analysis, we have chosen the simplest but most instructive type of branched polyelectrolytes, the star-branched polyelectrolyte. The degree of branching in this case is simply determined by the number of branches joined in one junction point.

After the description of our model in section 2, we consider the intramolecular screening by counterions in the dilute limit as manifested in the dependence of the star size on the number of branches (section 3). The screening by added salt and the dependence of the star conformation on the salt concentration are analyzed in section 4. In section 5, we consider the concentration effects in a salt-free solution of stars and we discuss the overlap threshold. Our conclusions are summarized in section 6.

2. Cell Model for a Solution of Polyelectrolyte Stars

We envisage a dilute solution of star-branched polyelectrolytes as an ensemble of spherical cells (analogous to the Wigner−Seitz cell[16]), each containing one polyelectrolyte star molecule localized at the center, Figure 1. The cell radius D equals half the average distance between the centers of neighboring stars, i.e. $D \sim c_P^{-1/3}$. Here and below, the polyelectrolyte concentration c_P is assumed to be below the overlap concentration. The star-shaped polyion (with a bare charge eQ) occupies the central region, $r < R$, of each cell. Here, r is the distance from the center of the cell and R is the average extension of branches. The periphery of the cell, $R < r < D$, corresponds to the interstar space in the solution.

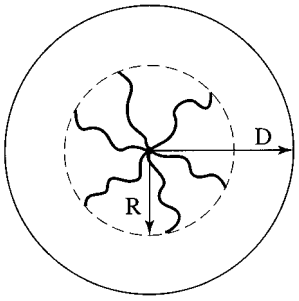

Figure 1. A polyelectrolyte star in a spherical cell. The star has f branches of N monomer units each. The cell radius is D, and the star occupies the central region within radius R.

The strength of the electrostatic field (and as a result the derivatives of the concentration profiles of all types of small ions) vanishes at the edge of the cell, at $r = D$. Polymer concentration effects in the dilute range are modeled by varying D.

The main molecular parameters of the polyelectrolyte star are the number of branches f, the number of monomers per branch N, and the fraction of charged monomers m^{-1}. Here, $m - 1$ is the number of uncharged monomers between two neighboring charges along the chain. The overall charge eQ of the star is then equal to efN/m, where e is the elementary charge.

The fraction m^{-1} of charged monomer units in the chain is assumed to be small. The Bjerrum length $l_B = e^2/k_BT\epsilon$ is of the order of a monomer size which is taken as the unit length. Here, ϵ is the dielectric constant of the solvent, T is the temperature, and k_B is the Boltzmann constant. The star branches are intrinsically flexible; i.e., the Kuhn segment length is also of order unity.

Because of the electroneutrality of the solution as a whole, the cell contains Q monovalent counterions. When salt is added, co-ions and counterions of the salt are also added in equal amounts.

2.1. Analytical Model. In the following, we will use a mean-field Flory-type approach for the analysis of the large-scale properties of a dilute salt-free solution of polyelectrolyte stars. The free energy can be split into various contributions

$$F = F_{\text{Coulombic}} + F_{\text{ions}} + F_{\text{conf}} + F_{\text{conc}} \qquad (1)$$

describing the Coulombic interactions between all charges (charged monomers and counterions), the translational entropy of counterions, the conformational entropy of the extended branches of the star, and the concentrational (osmotic) part describing the short-range interactions between uncharged monomers, respectively. We remark that, within the accuracy of excluded-volume terms, this mean-field model is equivalent to that used earlier.[13] A similar mean-field cell model has also been applied for ionic microgels by Kramarenko et al.[21]

The free energy given by eq 1 is a functional of the monomer and counterion density distributions. However, in order to analyze the dependence of the average star size R on parameters such as the number of branches f, the length of the branches N, the fraction

of charged monomers m^{-1}, and the cell radius D, we neglect spatial variations of these densities within the central region $r < R$ and in the peripheral region $R < r < D$. In other words, we define the free energy in eq 1 as a function of two variables: the radius of the star R and the actual (uncompensated) charge in this central region Q^*. Hence, we assume that $Q - Q^*$ counterions are retained by Coulombic attractions in this central region $r \leq R$, whereas the remainder of the counterions Q^* are distributed evenly in the region $R < r < D$.

As we assume the density of counterions (and the electrostatic potential) to have constant (but different) values inside and outside the star, the Coulombic term is[17]

$$F_{\text{Coulombic}}/k_{\text{B}}T = l_{\text{B}}\frac{Q^{*2}}{R}\vartheta\left(\frac{R}{D}\right) \tag{2}$$

where the function $\vartheta(x)$ is given by

$$\vartheta(x) = \frac{1}{10}\left[1 + \frac{5 - 9x + 5x^3 - x^6}{(1 - x^3)^2}\right]$$

The translational entropy term, giving the contributions of the translational entropy of ions inside and outside the star, is

$$F_{\text{ions}}/k_{\text{B}}T = (Q - Q^*)\ln\left(\frac{Q - Q^*}{V(R)}\right) + Q^*\ln\left(\frac{Q^*}{V(D) - V(R)}\right) \tag{3}$$

where $V(r) = (4\pi/3)r^3$.

The conformational entropy of the extended branches of the star can, in the Gaussian approximation, be written as

$$F_{\text{conf}}/k_{\text{B}}T = \frac{3fR^2}{2N} \tag{4}$$

For the nonelectrostatic osmotic contribution, we use the virial expansion

$$F_{\text{conc}}/k_{\text{B}}T = {}^1/_2 vfN\varphi_{\text{P}} + {}^1/_6 wfN{\varphi_{\text{P}}}^2 \tag{5}$$

where $\varphi_{\text{P}} = 3fN/4\pi R^3$, which is the volume fraction of polymer segments within the star volume and v and w are the dimensionless second and third virial coefficients, respectively. The former is related to the Flory–Huggins χ parameter as $v = 1 - 2\chi$. In a Θ solvent, the binary attraction of monomers compensates their excluded volume so that $v = 0$. Whereas linear polymers under Θ conditions exhibit Gaussian statistics, in strongly branched polymers the ternary repulsive interactions appear to be strong enough to induce swelling of the star even when $v = 0$.[18–20]

The values of Q^* and R are found from minimization of the free energy:

$$\left(\frac{\partial F(Q^*, R)}{\partial Q^*}\right)_{\text{R}} = 0 \tag{6}$$

$$\left(\frac{\partial F(Q^*, R)}{\partial R}\right)_{Q^*} = 0 \tag{7}$$

The result is

$$Q^* = \frac{R}{l_{\text{B}}}\frac{1}{2\vartheta(R/D)}\ln\left[\left(\frac{Q}{Q^*} - 1\right)\left(\frac{D^3}{R^3} - 1\right)\right] \tag{8}$$

$$R^3 = \frac{N}{3f}\left\{l_{\text{B}}Q^{*2}\left[\vartheta(R/D) - \frac{R}{D}\vartheta'(R/D)\right] + 3R\left[Q - \frac{Q^*}{1 - (R/D)^3}\right] - \frac{9f^2N^2}{8\pi R^2}\left(v + \frac{fN}{2\pi R^3}w\right)\right\} \tag{9}$$

where $\vartheta'(x) \equiv \mathrm{d}\vartheta/\mathrm{d}x$.

These two equations describe both the star size R and the uncompensated charge Q^* inside R as a function of the bare charge Q, the number of branches f, the branch length N, and the cell size D.

2.2. Numerical SCF Model. The numerical SCF approach is based on the Scheutjens–Fleer (SF) algorithm proposed earlier for neutral polymers at interfaces[22,23] and extended to account for the electrostatics on a Poisson–Boltzmann level.[24] Some information on the method is given below; for full details, one should consult the original literature.

The SF–SCF approach uses a lattice which facilitates accounting for the volume of all molecular components. A lattice cell with the size of the Bjerrum length can be occupied either by a solvent molecule S, by a polymer segment P, or by a mobile ion. We assume that there are two types of ions in the system: co-ions, Cl^-, and counterions, Na^+ (polymer segments are assumed to be negatively charged). The lattice cells are arranged in an array of concentric spherical shells (or "layers") numbered as $z = 1, ..., M$; the outer surface of the zth layer is at the distance $r = zl_{\text{B}}$ from the center. The total cell radius is given by $D = Ml_{\text{B}}$. The volume of the system within the shell number z is given by $V(z) = 4\pi z^3{l_{\text{B}}}^3/3$ and a layer at coordinate z contains $L(z) = (V(z) - V(z-1))/{l_{\text{B}}}3 = 4\pi(z^2 - z + {}^1/_3)$ lattice sites. The dimensionless inner area a_{i} and outer area a_{o} of a lattice site in layer z are given by $a_{\text{i}}(z) = 4\pi(z-1)^2/L(z)$ and $a_{\text{o}}(z) = 4\pi z^2/L(z)$, respectively. These quantities determine the so-called a priori step probabilities, $\lambda(z, z')$, for steps from layer z to z', where z' takes the values $z - 1$ (to the inner layer), $z + 1$ (to the outer layer), and z (within the same layer). The step probabilities are given by $\lambda(z, z-1) = a_{\text{i}}(z)/6$, $\lambda(z, z+1) = a_{\text{o}}(z)/6$, and $\lambda(z, z) = 1 - \lambda(z, z+1) - \lambda(z, z-1)$, respectively.

The SCF formalism features the particle potentials $u_x(z)$ which are conjugated to the volume fractions $\varphi_x(z)$. These volume fractions are related to the local concentrations as $\varphi_x(z) = c_x(z){l_{\text{B}}}^3$. Subscript x is used to refer to the various types of particles $x = S, P, Na^+, Cl^-$. The functions $u_x(z)$ and $\varphi_x(z)$ are mutually dependent and are, for a given particle type, only functions of the z coordinate. Hence, all the local properties of the system are preaveraged over the angular coordinates (the spherical approximation). The total potential of a particle of type x comprises three terms:

$$u_x(z) = u'(z) + k_{\text{B}}T\sum_y \chi_{xy}(\langle\varphi_y(z)\rangle - \varphi_y^{\text{b}}) + \nu_x e\psi(z) \tag{10}$$

The first term is coupled to the incompressibility constraint $\sum_x \varphi_x(z) = 1$. The second term gives the short-range interactions, parametrized by Flory–Huggins interaction parameters χ_{xy} between particle types x and y; this interaction term depends on the volume fraction

of the components. The term $\langle\varphi_y(z)\rangle$ is the site-average volume fraction, which is equal to $\lambda(z, z-1)\,\varphi_y(z-1) + \lambda(z, z)\,\varphi_y(z) + \lambda(z, z+1)\,\varphi_y(z+1)$ (note that the site fraction causes the potential to be nonlocal and geometry dependent). The quantity φ_y^b in eq 10 is the concentration of monomers of type y in the bulk. The third term accounts for the electrostatic contributions. The local charge $q(z)$ per lattice layer is given by $q(z) = e\sum_x \nu_x\varphi_x(z)$, where e is the elementary charge and ν_x the valence of the particle of type x. The local electrostatic potential, $\psi(z)$, is related to the local charge density, $q(z)$, via the Poisson equation.

In order to obtain the density profiles $\varphi_x(z)$ from the segment potentials $u_x(z)$, one has to evaluate all possible and allowed conformations of the molecules in the potential field. In the special case of a polymeric star, one has to consider the grafting constraint present on the first segments of each arm. In a first-order Markov approximation, one can compare the chain conformations of one arm of the star with segments $s = 1, ..., N$ with the path of a diffusing particle in an external field that starts in (or near) the center of the coordinate system and ends up somewhere in the system at a time t (=N). The corresponding diffusion equation features end-point distribution functions $G_P(z, s|z^*, 1)$ for the statistical weight of finding a chain fragment that starts with segment $s = 1$ at z^* (grafting point) and ends in layer z with segment s and correspondingly $G_P(z, s|N)$ for the statistical weights of all possible and allowed conformations, with the specification that segment $s = N$ can be anywhere in the system and again segment s is at coordinate z. Hence, $G_P(z, s|N)$ is the sum of $G_P(z, s|z', N)$ over all z'. The end-point distribution functions obey, as already mentioned, the diffusion equation which, in discrete notation, can be written as

$$G_p(z, s|z^*, 1) = G_p(z)\langle G_p(z, s-1|z^*, 1)\rangle$$

$$G_p(z, s|N) = G_p(z)\langle G_p(z, s+1|N)\rangle \qquad (11)$$

These propagator relations are started by the condition that a "walk" of one segment long should be weighted by the free segment distribution function: $G_P(z, N|N)$ and $G_P(z)$ for all z and $G_P(z^*, 1|z^*, 1) = G_P(z^*)$ (grafting condition). The segmental weighting factor $G_P(z)$ is defined as $\exp(-u_P(z)/k_BT)$. The segment densities follow from the composition law:

$$\varphi_p(z, s) = C_p\frac{G_p(z, s|z^*, 1)\,G_p(z, s|N)}{G_p(z)} \qquad (12)$$

Here, the factor $G_P(z)$ in the denominator corrects for the double counting of the Boltzmann weight for segment s in the nominator. The normalization factor C_P is fixed by the number of arms f in the system:

$$C_p = \frac{fN}{\sum_{z=1}^{M} L(z)\,G_p(z, N|z^*, 1)} \qquad (13)$$

The grafting coordinate of the arms of the star, z^*, is chosen such that $L(z^*-1) < f < L(z^*)$. The density distributions of all monomeric components $x \in \{S, Na^+, Cl^-\}$ follow directly from the above formalism; eq 12 now reduces to $\varphi_x(z) = \varphi_x^b G_x(z)$. Note that $\varphi_{Na^+}^b = \varphi_{Cl^-}^b$ as the electrostatic potential vanishes in the bulk of the solution.

The set of equations as presented in this section is closed but should be complemented by boundary conditions. As the cell is electroneutral as a whole, we set the "reflecting" boundary conditions at $z = M$, which guarantees that there are no gradients present in the z direction between $z = M$ and $z = M + 1$; i.e., $\psi(M+1) = \psi(M)$, $u_x(M+1) = u_x(M)$, etc.

The above set of equations are solved iteratively by a Newton-like method. This results in radial distributions of overall monomer densities, P, S, Na^+, Cl^-, as well as, e.g., the densities of end segments and all the interior segments, the segment potentials, and the electrostatic potential. It is also easy to obtain measures for the size of the star, such as the first moment of the distribution of end segments:

$$R = \frac{\sum_{z=z^*}^{M} L(z)\,(z - z^*)\,\varphi_p(z, N)}{\sum_{z=z^*}^{M} L(z)\,\varphi_p(z, N)} \qquad (14)$$

Parameters are taken as simple as possible: $\chi_{xy} = 0$ when both x and y are not P, in a good solvent $\chi_{Py} = 0$ and under Θ-conditions $\chi_{Py} = 0.5$. The valences are defined as follows $\nu_S = 0$, $\nu_{Na^+} = 1$, $\nu_{Cl^-} = -1$, and $\nu_P = m^{-1}$. The last statement means that every monomer has the same charge, which is between 0 and -1.

3. Dilute Salt-Free Solution: Charge Renormalization and Intrinsic Screening

We start with the analysis of the conformation of a polyelectrolyte star in a dilute, salt-free solution. The values of R and Q^* follow from solving the two implicit equations (8) and (9) simultaneously. Previously, scaling relations for the star size as a function of the number of branches, the fraction of charged monomers, and the branch length have been derived.[13] In this section, we compare these scaling predictions to the analytical model as described in the previous section and to the numerical SCF results.

As follows from eq 8, in the dilute limit $D \gg R$, the distribution of counterions in the solution strongly depends on the ratio between the bare star charge eQ and the star radius R.

At $Q \ll R/l_B$, the Coulombic attraction of counterions to the star is relatively weak and the translational entropy favors a uniform distribution in the whole available space of the solution. This means that, at $D \gg R$ (dilute limit), the average fraction of counterions localized in the volume occupied by the star is small and charged branches interact by unscreened Coulombic repulsion. This is the case for stars with a small number of branches, $f \ll f^*$, where f^* corresponds to the crossover between the unscreened and the intrinsically screened stars (see below). As has been shown in the literature, $f^* \cong m^{1/2}l_B^{-1}$.[13,14] The stars with $f \ll f^*$ shall be referred to as "unscreened stars". The asymptotic expression for the dimensions of the unscreened star can be obtained from eqs 8 and 9 if the last two terms in eq 9 describing the contribution of the excluded-volume interactions are

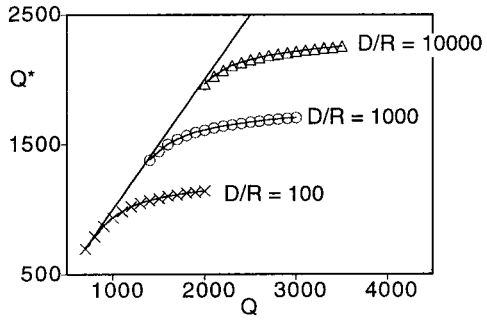

Figure 2. Charge renormalization effect: an effective (uncompensated) charge Q^* within the radius R as a function of the bare (immobilized) charge Q calculated from eq 8 for different values of the cell size. $D/R = 10^2, 10^3, 10^4$; $R = 100$.

negligibly small compared to the other terms and $f \ll f^*$. Balancing then the unscreened Coulombic repulsion, so $Q^* = Q$, with the conformational entropy losses in extended branches gives the result that the star size grows with increasing number of branches as[13]

$$R \cong N m^{-2/3} l_B^{1/3} f^{1/3} \tag{15}$$

As soon as the excluded-volume interactions play an important role, the effective exponent for the f dependence of the star size is somewhat smaller. We remark that the size of a neutral star grows due to intrabranch steric repulsion with increasing number of branches as $R \sim f^{1/5}$ or $R \sim f^{1/4}$ under good or Θ-solvent conditions, respectively, instead of $R \sim f^{1/3}$ as for polyelectrolyte stars.[18−20]

In the opposite limit, $Q \gg R/l_B$ (corresponding to the screened stars), the Coulombic attraction becomes strong enough to win the competition with the translational entropy so that the distribution of counterions in the solution becomes strongly nonuniform. Most of the counterions remain in the volume occupied by the star, and their concentration is much larger there than the average concentration in the solution, while the concentration of "free" counterions in the interstar volume is much smaller than this average value.

The average number of "free" counterions, given by the uncompensated charge Q^* in the volume occupied by the star, is determined by eq 8 and presented in Figure 2 as a function of the bare charge Q. As follows from the figure, Q^* equals Q for small values of Q, whereas at large values of the bare charge, the effective uncompensated charge Q^* grows only logarithmically with increasing Q, so that the dependence of Q^* on Q levels off. In the range of large bare charges, $Q \gg R/l_B$, the uncompensated charge within the volume of the star remains proportional to R/l_B (i.e., it is much smaller than the bare charge Q). This means, in turn, that most of counterions remain effectively trapped in the interior of the star by the Coulombic attraction and only a small fraction of them are released into the bulk of the solution. This concept is known as charge renormalization and was first proposed by Alexander et al.[25] for salt-free solutions of charged colloidal particles and later by Pincus[26] for polyelectrolyte brushes.

The physical meaning of the charge renormalization threshold, $Q^* \cong R/l_B$, is transparent: the counterions are pulled inside the star by the Coulombic force and compensate the charge of the star unless the energy of the Coulombic attraction $e^2Q^*/\epsilon R$ is smaller than the thermal energy k_BT.

With increasing number of branches, f, the Coulombic interactions become stronger because the size of the star in the unscreened regime grows as $\sim f^{1/3}$, according to eq 15, whereas the bare charge of the star grows as $\sim f$. For stars with a large number of branches, $f \gg f^*$, Q is no longer much smaller than R/l_B and most of the counterions are retained in the interior of the star. These counterions ensure partial screening of the Coulombic repulsion between charged branches. In the limit $f \gg f^*$ the terms $\sim Q^*$ in the right-hand side of eq 9 are negligibly small. If we ignore the nonelectrostatic (excluded-volume) interactions, we derive from eq 9 the dependence of the size of the star on of the number of arms in the screened regime:

$$R(f) \cong N m^{-1/2} \tag{16}$$

which indicates that the size of the many-armed star becomes independent of the number of branches. Equation 16 does not take into account the incomplete compensation of the star charge by counterions trapped in the intrastar space, i.e. the presence of a small fraction of counterions in the interstar space of the solution. If the latter is taken into account, a weak (logarithmical) growth instead of a plateau in the $R(f)$ curve is expected. This regime for $Q \gg R/l_B$ is called the osmotic regime. The reason is that eq 16 can be obtained also on the basis of "osmotic" arguments:[13,26] the extensional Coulombic force applied to the branches of the star is proportional to the excess osmotic pressure due to counterions trapped inside the star by the attractive Coulombic force. The balance between this osmotic pressure and the conformational free energy penalty for the extension of branches, eq 4, results in eq 16.

The alternative set of arguments leading to eq 16 is based on the concept of intrinsic screening length. We introduce the Debye screening length, κ^{-1}, as

$$\kappa^{-1} \cong (l_B c)^{-1/2} \tag{17}$$

where c is the concentration of mobile ions. In this paper, we use two different Debye screening lengths, the intrinsic screening length, κ_i^{-1}, and the screening length caused by added salt, κ_s^{-1}. κ_i^{-1} is defined as $(l_B c_i)^{-1/2}$, where c_i is the concentration of counterions in the intrastar space. It is easy to prove that $\kappa_i^{-1} \ll R$; i.e., Coulombic interactions inside the star are screened on a scale much smaller than the star radius if the condition $f \gg f^*$ applies. This is the basis of the local electroneutrality approximation, according to which there is a local compensation of the immobilized charge on the branches by counterions on the scales larger than κ_i^{-1}.

The effect of the screened Coulombic repulsion of the charged monomers on the large-scale conformational properties of the star polymer is equivalent to that of the short-range binary repulsion (excluded-volume interactions) and can be formally described using the effective (electrostatic) second virial coefficient[27]

$$v_{eff} \cong l_B \kappa^{-2} m^{-2} \tag{18}$$

The factor m^{-2} reflects the fact that only a fraction m^{-1} of monomers is charged. The size of the star, which is dominated by short-range binary repulsive interaction

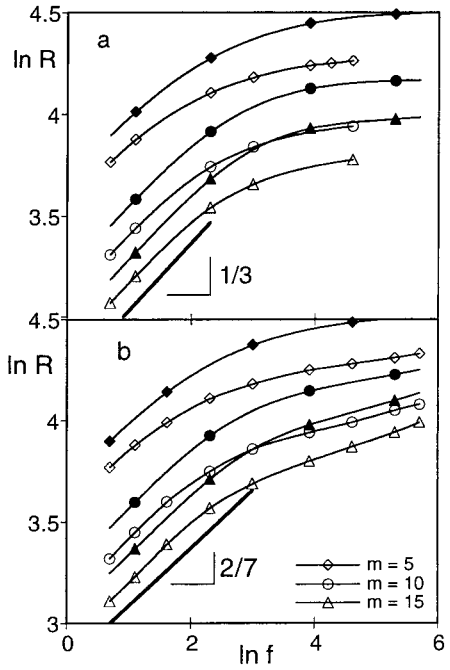

Figure 3. Star size R as a function of the number of branches f (in double-log coordinates) in a salt-free solution under Θ (a) and good (b) solvent conditions for $N = 200$ and for $m = 5$ (diamonds), 10 (circles), and 15 (triangles). The curves with the closed symbols correspond to the solution of eqs 8 and 9, while the lines with the open symbols correspond to results of SCF calculations at $\varphi_s^b = 10^{-7}$ and $D = 150$. The bold lines show the slopes predicted by scaling.[13]

between monomers (good solvent conditions), is given by[18−20]

$$R \cong N^{3/5} f^{1/5} v^{1/5} \tag{19}$$

Taking into account the definition of κ_i^{-1} and the local electroneutrality condition $c_i \cong c_P/m$, we arrive at the known result eq 16.

According to eq 16, the star size is expected to be virtually independent of the number of branches in a certain range of f. Therefore, with increasing number of branches, the monomer concentration and, as a result, the relative importance of the nonelectrostatic interactions between uncharged monomers increase. At a very large number of branches, $f \gg (N/m)^2$, these nonelectrostatic interactions become dominant.[13] Obviously, this regime is attainable only for very weakly charged, $m \gg 1$, stars.

If the concentrational contribution described by the last term in eq 9 is neglected, then eqs 8 and 9 interpolate between two asymptotic limits given by eqs 15 and 16, which give the radius R for a star with small and large numbers of arms, respectively.

The dependencies of the star size R on the number of branches f have been calculated with the numerical SCF model at low ionic strength of the solution, $\varphi_{Na}^b + = \varphi_{Cl^-}^b = 10^{-7}$, and by simultaneous solution of eqs 8 and 9 of the analytical model. The results are shown in Figure 3.

As expected from eqs 15 and 16, ln R, increases linearly with ln f for the stars with small numbers of branches and levels off for the many-armed stars. The remaining growth is mainly due to the increasing importance of the nonelectrostatic interactions of uncharged monomers and is more pronounced in a good solvent (Figure 3b) than in a Θ solvent (Figure 3a).

The initial slope of ln R vs ln f curves is close to $^1/_3$ (eq 15) in a Θ solvent ($m = 5$, 10, 15) and is close to $^2/_7$ in a good solvent, as predicted earlier.[13] For $m = 2$ (not shown in the figure), the initial slope is significantly smaller because the fraction of charged monomers is large enough to induce intrinsic screening by counterions even at small values of f ($f^* \sim m^{1/2} \sim 1$ in this case).

The two methods of calculation give the same trends, although the analytical approach systematically gives a larger star radius than the SCF calculations. This difference is not surprising in view of the uniform charge density approximation used in our analytical model. The latter approximation becomes especially poor in the interstar region where the actual distribution of counterions is strongly nonuniform. This nonuniform distribution is fully taken into account in the SCF calculations.

It is instructive to analyze the m dependence of the size of stars for different values of f. Figure 4 shows a double-logarithmic plot of R as a function of m. We see that, with increasing f, the absolute value of the slope of ln R vs ln m curves systematically decreases from ≅0.66 to ≅0.5 in a Θ solvent and from ≅0.57 to ≅0.4 in a good solvent, which is in accordance with the prediction of eqs 15 and 16 and the results of the scaling analysis.[13] This gives thus an indication that the (asymptotic) unscreened and osmotic regimes at small and large f, respectively, really exist.

The SCF method allows us to get a better insight into the intrinsic structure of the star through the analysis of the radial distribution of the monomer and counterion densities.

Figure 5 shows the radial decay of the monomer density in log−log coordinates for stars with different numbers of branches ($f = 3$, 20, 100). We see that, in a wide range of r, corresponding to the internal region $r < R$, the slope is close to −2, which indicates a uniform extension of the branches. This is expected[14] because $R \sim N$, according to eqs 15 and 16, for both unscreened and osmotic stars.

The extension vanishes (i.e., the local tension vanishes) at the free ends of branches. Figure 6 presents the radial distribution of the free chain ends, normalized for one branch, in stars with different numbers of branches.[28] The free ends are localized in a relatively narrow range near the edge of the star. The fluctuations in the overall extension of branches are nearly Gaussian in stars with a relatively small number of branches ($f \leq 50$; see Figure 6). With increasing number of branches, the position of the maximum of the distribution shifts to larger r, which reflects an increase in the overall extension. However, as we have discussed above, for many-armed stars the average star size (i.e., the position of the maximum in the $\varphi_e(r)$ curve) is virtually independent of the number of branches. This feature is clearly demonstrated in Figure 6. It is important to note that the distribution of the free ends is wide for large f; its shape becomes asymmetric and is reminiscent of the distribution of free chain ends in a planar polyelectrolyte brush.[29] In other words, near the edge of a many-armed star, the effect of curvature is weak and the structure of the peripheral region of the star resembles that of a planar polyelectrolyte brush. As a rough estimate for the onset of the development of the asymmetry of the $\varphi_e(r)$ distribution, we can use the condition $\kappa_i^{-1} \leq N^{1/2}$,

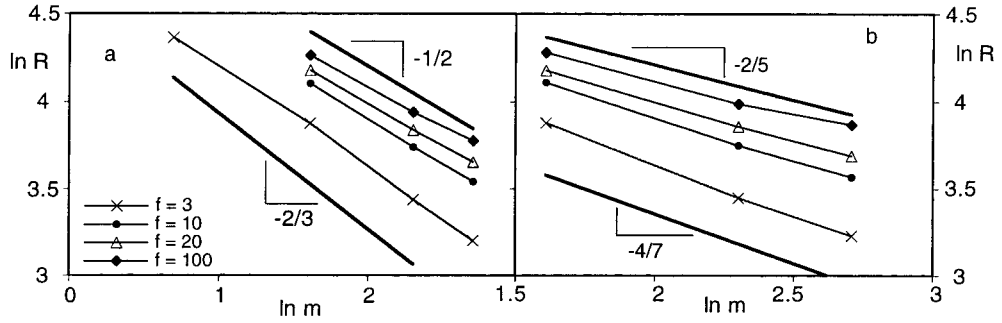

Figure 4. Star size R as a function of m (in double-log coordinates) for $f = 3$ (crosses), 10 (dots), 20 (triangles), and 100 (diamonds), under Θ (a) and good (b) solvent conditions. $N = 200$, $D = 150$, and $\varphi_s^b = 10^{-7}$. The bold lines show the slopes predicted by scaling.[13]

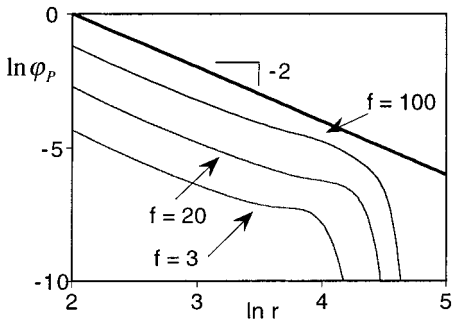

Figure 5. Monomer density profile $\varphi_P(r)$ (in double-log coordinates) for stars with different numbers of branches f (Θ-solvent conditions, $N = 200$, $m = 5$, $D = 150$, $\varphi_s^b = 10^{-7}$). The bold line indicates the slope -2 corresponding to a uniform extension of the branches.

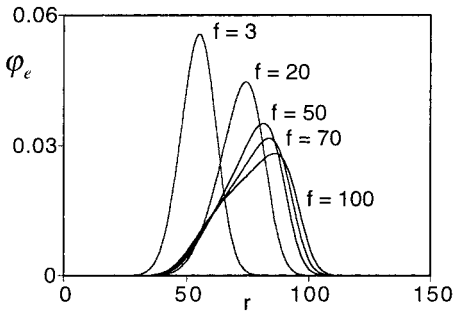

Figure 6. Radial distribution $\varphi_e(r)$ of the end monomers of the star (normalized for one branch) for stars with different numbers of branches f (Θ-solvent conditions, $N = 200$, $m = 5$, $D = 150$, $\varphi_s^b = 10^{-7}$).

which implies that the electrostatic field is screened on the lengths smaller than the range of the Gaussian fluctuations of extended branches of the star. This condition results in $f \geq f^*N/m$. For the set of parameters used in Figure 6, we calculate that the number of arms should be larger than 40, which agrees with the observation noted earlier. At larger f, the intrinsic screening length κ_i^{-1} at the edge of the star is smaller than the range of Gaussian fluctuations of the extension of branches and we expect quasi-planar behavior of the periphery of the star. We mention the direct analogy between this observation and that in the literature,[30] where the intrinsic structure of neutral polymer stars was studied by the numerical SCF method.

Figure 7 gives an illustration of the distribution of counterions inside the star and in the bulk of the solution around the star. In order to illustrate the degree of localization of counterions in many-armed stars, we present both the counterion and the polymer

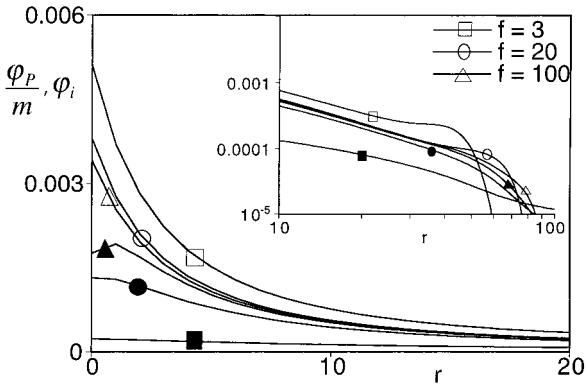

Figure 7. Radial distribution of charged monomers and counterions (normalized for one branch) in stars with different numbers of branches f. The curves with the closed symbols correspond to the distribution of counterions φ_i; those with the open symbols give the monomer distribution φ_P/m (Θ-solvent conditions, $N = 200$, $m = 5$, $D = 150$, $\varphi_s^b = 10^{-7}$).

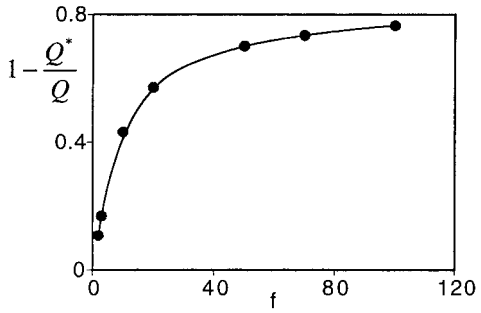

Figure 8. Fraction of counterions localized inside the star (at $r < R$) as a function of the number of branches f (Θ-solvent, $N = 200$, $m = 5$, $D = 150$, $\varphi_s^b = 10^{-7}$).

densities (the latter is divided by m). Both densities are normalized for one branch. As follows from Figure 7, at small f, the counterions spread fairly uniformly over the cell volume. With increasing f, the counterions become more and more localized inside the star. At large f, the radial profiles of counterions and charged monomers inside the star approach each other, which illustrates the local electroneutrality in the many-armed stars. The deviation from local electroneutrality becomes significant in the peripheral regions close to the edge of the star; see insert in Figure 7. The local concentration of monomers (and of counterions) is such that the local screening length becomes comparable to the total star size.[14]

Figure 8 presents the fraction of "trapped" counterions (localized at $r \leq R$, where R is the average end position) as a function of f. With increasing f, the fraction of

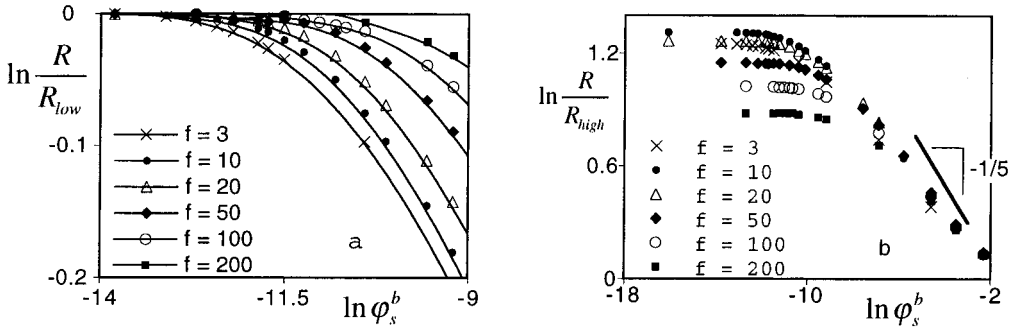

Figure 9. Star size R as a function of the volume fraction of salt in the bulk φ_s^b (in double-log coordinates) for stars with different numbers of branches f under Θ-solvent conditions ($N = 200$, $m = 5$). In Figure 9a, the star size R is normalized to its value at $\varphi_s^b = 10^{-7}$, R_{low}, while in Figure 9b, it is normalized to its value at $\varphi_s^b = 10^{-1}$, R_{high}. The bold line shows the slope predicted by scaling.[14]

trapped counterions systematically increases and tends to 1 for large f. This constitutes direct proof of the localization of counterions in many-armed stars, i.e. the existence of the osmotic regime.

4. Dilute Solution: Screening by Added Salt

The addition of low-molecular-weight salt to a solution of branched polyelectrolytes results in additional screening of the Coulombic repulsion between charged branches of the stars and in a deswelling with increasing salt concentration.

As we have demonstrated in the previous section, the intramolecular Coulombic repulsion in many-armed stars is already partially screened in the salt-free solution by counterions localized preferentially in the intrastar space. The degree of localization of counterions and the effect of intrinsic screening depend strongly on the number of branches. Hence, the effect of additional screening by salt is expected also to be strongly dependent on the number of branches in the star.

As was discussed earlier,[14] the larger the number of branches, the higher the salt concentration required to affect the conformation of the star. In other words, the salt concentration in the bulk of the solution c_s^b must exceed significantly the intrinsic concentration of counterions $c_i \cong c_P/m$ in order to affect the star conformation (i.e., to induce deswelling of branches). So, at small salt concentration, $c_s^b \ll c_i$, the intramolecular screening is dominated by counterions, while in the limit of high salt, $c_s^b \gg c_i$, both co-ions and counterions contribute significantly to the screening of the intrastar Coulombic repulsion.

The size of the star in the salt-dominance regime can be derived using the same mean-field arguments as used for the star screened by counterions only. The effective (electrostatic) second virial coefficient, $v_{eff} \cong l_B\kappa^{-2}\, m^{-2}$, is determined by the bulk screening length, $\kappa_s^{-1} \cong (lc_{Bs}^b)^{-1/2}$, and substitution into eq 19 gives

$$R \cong N^{3/5} f^{1/5} m^{-2/5} (c_s^b)^{-1/5} \qquad (20)$$

The same result has been obtained in the literature[14] on the basis of osmotic arguments by balancing elasticity of the branches with the differential (excess) osmotic pressure of all types of mobile ions inside and outside the star.

Figure 9 presents the results of SCF calculations for the star size R as a function of the bulk volume fraction of salt $\varphi_s^b \equiv \varphi_{Na^+}^b \equiv \varphi_{Cl^-}^b$ in the range of φ_s^b from 10^{-7} to 10^{-1} corresponding to the variation of the Debye screening length (measured in the monomer lengths) from approximately 200 to unity. The number of monomers per branch, N, is equal to 200; the fraction of charged monomers is set equal to 0.2 (i.e., $m = 5$). Different curves correspond to different numbers of branches f, which is varied over a wide range, $3 < f < 200$.

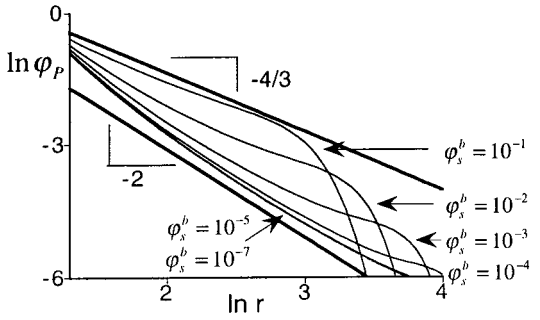

Figure 10. Monomer density profile (in double-log coordinates) of a star with $f = 20$ branches under Θ-solvent conditions at different salt concentrations (shown in the figure) ($N = 200$, $m = 5$, $D = 1500$). The bold lines show the slopes predicted by scaling.[14]

All the curves in Figure 9a are normalized to the value at "low" salt (at $\varphi_s^b = 10^{-7}$ in our calculations). At large f, there is a well-developed plateau at small salt concentration where $R = R_{low}$, corresponding to a predominance of counterions in the intramolecular screening. With increasing salt concentration, the salt starts to contribute to the screening and gradual deswelling of stars occurs. The larger the number of branches f in the star, the higher the salt concentration where the onset of this deswelling is found.

In the limit of large salt concentration (the salt-dominance regime), ln R decreases almost linearly with φ_s^b, as demonstrated in Figure 9b, where the sizes of the stars are normalized to their values at "high" salt concentration $\varphi_s^b = 10^{-1}$. The slope is found to be close to $-1/5$, as predicted by eq 20.

Figure 10 presents the evolution of the monomer density profile (in log−log coordinates) for a star with $f = 20$ at several ionic strengths. The slope of ln $\varphi_P(r)$ vs ln r curves in the central part of the star progressively decreases from around -2 in the salt-free regime to around $-4/3$ at high salt concentration. The power law $\varphi_P \sim r^{-4/3}$ for the radial decay of the monomer density is typical for a star swollen by short-range binary repulsive interactions between the monomers[31] and has been predicted for the salt-dominance regime.[14]

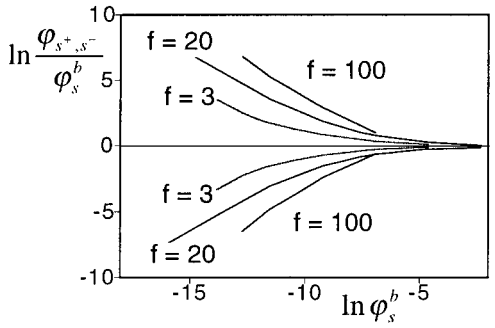

Figure 11. Ratios of the average concentrations of co-ions and counterions inside the star to the bulk value as a function of the volume fraction of salt in the bulk φ_s^b (in double-log coordinates), for stars with different numbers of branches f under Θ-solvent conditions ($N = 200$, $m = 5$, $D = 150$).

Figure 11 shows the relative volume fractions of co-ions and counterions inside the star as a function of φ_s^b for different values of f. For a star with a small number of arms and low φ_s^b, the concentration of ions inside the star is relatively close to the bulk value. For large f, the concentration of counterions inside the star is much larger than the bulk volume fraction φ_s^b, but the difference becomes smaller as φ_s^b increases and the salt-dominance regime is approached.

5. Concentration Effects in Dilute Solution: Star Contraction and Overlap Threshold

The behavior of charged macromolecules with increasing concentration in the solution is qualitatively different from that of neutral ones because of the long-range character of intramolecular Coulombic interactions and the screening effect of counterions. This difference is most pronounced in a salt-free case. In the high-salt-concentration regime, strongly screened Coulombic interactions are equivalent to short-range excluded-volume interactions. In the latter case, charged polymers behave like neutral ones under good solvent conditions (see previous section).

In dilute solutions (and in a good solvent), neutral polymers are swollen due to short-range intramolecular excluded volume repulsions of monomers. This swelling is the same (with the accuracy of weak concentrational effects) in the whole range of dilute solutions, i.e. at all concentrations below the overlapping threshold c^*. At concentrations above c^*, the intramolecular excluded-volume repulsion becomes partially screened due to other polymers. This screening becomes stronger and, correspondingly, the polymer deswells as the concentration of the solution increases. The chains approach their Gaussian (ideal) dimensions as the volume fraction (the concentration of polymer in the solution) approaches unity. For neutral polymers, screening of intramolecular interactions occurs only above c^*, i.e. in the semidilute regime. The overlap threshold is thus determined by the polymer size R in the dilute solution[32] as $c^* \cong N/R^3$. Concentration effects in solution of neutral polymer stars have already been extensively discussed.[18,20]

The swelling of charged polymers in dilute solution is determined by the intramolecular Coulombic repulsion. Due to the presence of counterions, which are spread all over the volume of the solution because of entropic factors, this intramolecular repulsive interaction becomes progressively screened with increasing solution concentration even below the geometrical overlapping threshold for polyions. With increasing concentration of polyelectrolytes (and of the counterions) in the solution, the corresponding screening length becomes progressively smaller. The intrachain repulsion becomes weaker, and as a result, deswelling of polyelectrolytes occurs.

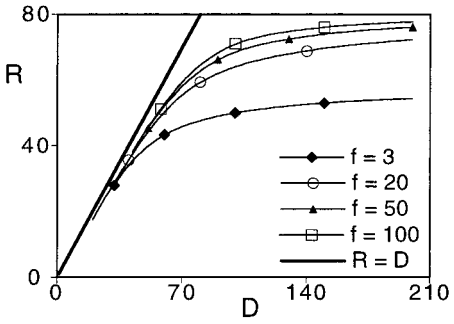

Figure 12. Star size R as a function of the cell radius D for different numbers of branches f (Θ-solvent conditions, $N = 200$, $m = 5$, $\varphi_s^b = 10^{-7}$). The "confinement" line $R = D$ is shown for comparison.

As discussed in section 3, the distribution of counterions in dilute solutions of branched polyelectrolytes is strongly inhomogeneous: the local density of counterions in the intramolecular space is larger than the average in the solution. This inhomogeneity becomes more pronounced with increasing degree of branching and becomes extreme (trapping of most of counterions) in solutions of many-armed stars. Hence, one can expect the following: (i) Polyelectrolyte molecules in a salt-free solution exhibit considerable deswelling with increasing concentration of polyelectrolytes below the overlapping threshold. (ii) The overlapping threshold is determined not by the polyelectrolyte size in the highly dilute limit but by the actual (much smaller) size which polyelectrolytes attain at the crossover between dilute and semidilute regimes. (iii) The deswelling induced by an increase of the solution concentration in the dilute regime is more pronounced for weakly branched polyelectrolytes; strongly branched ones are less sensitive to the solution concentration below the overlap threshold.

The last statement is the most important for us and is based on the fact that the concentration of counterions in the intermolecular space in a dilute solution of strongly branched polyelectrolytes is low in comparison to their intramolecular concentration.

In order to check these predictions, we have performed SCF calculations for the stars with different numbers of branches in a cell with a variable radius D.

The polymer density and the free-end distributions as well as the counterion distributions were calculated in order to get insight into the conformational changes which occur in a polyelectrolyte star with increasing concentration of the solution in the dilute regime (below the overlap threshold).

Figure 12 presents the average star size as a function of the cell radius D for $f = 3$, 20, 50, 100 and for $N = 200$ and $m = 5$. The bold line $R = D$ indicates the regime of "geometrical confinement" of the star in a cell corresponding to the close packing of stars in the solution. All the stars exhibit a significant decrease in size with decreasing D (increasing concentration) in the range $R \leq D$, i.e. $D \geq D^*$. Here we define the cell size D^* in analogy to the overlapping concentration of the solution c^*; this means that for D^* the star size R is

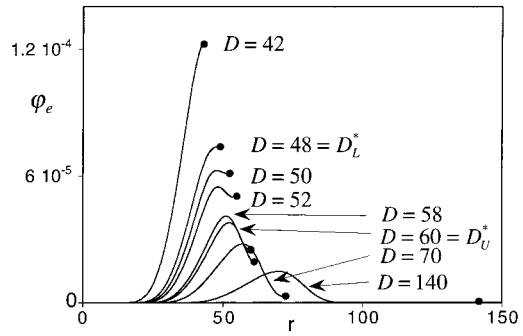

Figure 13. Example of the radial distribution of the end monomers $\varphi_e(r)$ for a star with $f = 20$, $N = 200$, $m = 5$, $\varphi_s^b = 10^{-7}$, Θ-solvent conditions, at different cell sizes D. The dots denote the end of the cell.

the same as the shell size D^*, $R(D^*) \cong D^*$. In order to obtain a better estimate for D^*, we have to analyze the evolution of the star intrinsic conformational structure with increasing solution concentration (decreasing D). From Figure 13, presenting the radial distribution of the free ends of a star, it follows that roughly three stages of the star contraction with decreasing D can be distinguished.

In the first stage, $D \gg R$, the star size decreases due to enhanced screening of intrastar repulsion by counterions which are progressively pushed into the intrastar volume as the overall available volume of the cell decreases. The maximum of the end-segment density distribution becomes progressively displaced to smaller r but retains its symmetrical (Gaussian) shape. In Figure 13, this is the case for $D \geq 70$.

However, the star size decreases with decreasing D not as rapidly as the cell radius, and at sufficiently small D, the right wing of the end-monomer distribution becomes truncated at the cell edge, $r = D$, and the distribution loses its symmetry. In fact, this marks the beginning of overlapping of stars in the solution and corresponds to the crossover between dilute and semidilute regimes. With decreasing D, the right wing of the distribution becomes more and more narrow and the maximum of the distribution becomes higher and approaches the cell edge.

Finally, upon a further decrease in D, the maximum (and the right wing) in the distribution disappears and the density of end segments becomes a monotonically increasing function from the center of the cell to the periphery (this is the case for $D \leq 48$ in Figure 13). This last regime corresponds obviously to the geometrical confinement of the star in the cell.

It is natural to associate the second stage of contraction, when the symmetry of the free-end distribution is already perturbed by the presence of the cell wall at $r = D$ but the maximum of the distribution is still localized at $r < D$, with the crossover region between dilute and semidilute solutions. For the conditions of Figure 13, this is the case for $50 \leq D \leq 60$. Hence, we can estimate D^* from above using the condition $D^* - R(D^*) \cong \Delta$, where Δ is the width of the free-end distribution. The lower estimate for D^* is given by the condition of the disappearance of the maximum in the free-end distribution. The upper estimate for D^* is given by the condition that the volume fraction of the end segments at D is half the value of the maximum; i.e., $\varphi_{e,max} = 2\varphi_e(D)$. The upper and the lower estimates for D^* are referred to as D_U^* and D_L^*, respectively; both are indicated in Figure 13.

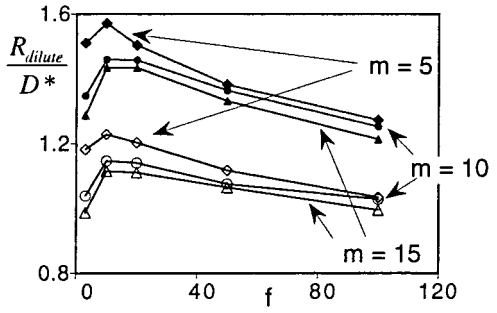

Figure 14. Relative magnitude of the maximal star contraction in the dilute regime, R_{dilute}/D^*, as a function of the number of branches f for different m, which are indicated in the graph (Θ solvent, $N = 200$, $\varphi_s^b = 10^{-7}$). The open symbols refer to D_U^* and the closed symbols to D_L^*.

Of course, this difference is only important for finite N. For sufficiently long branches, the width, $D_U^* - D_L^*$, of this crossover regime is relatively small (in comparison to the overall star size or to D^*) and the difference between lower and upper estimates for D^* becomes irrelevant.

Figure 14 presents the ratio R_{dilute}/D^*, where R_{dilute} is the star size at infinite dilution, thus for $D = \infty$. R_{dilute}/D^* characterizes the magnitude of contraction of the star in the dilute regime as a function of the number of branches in the star f. In the calculations, it is not possible to take D infinitely high, so D is taken 200. In accordance with our expectations for many-armed stars, the larger the number of branches in the star, the less sensitive the polyelectrolyte star size to the concentration increase in the dilute regime. For a many-armed star, the magnitude of this contraction is not large. We expect that, in the limit $f = \infty$, D^* tends to the star size in a highly dilute solution. An opposite trend, i.e. an increase of the ratio R_{dilute}/D^* for the stars with small numbers of branches, is remarkable.

In order to analyze the dependence of D^* on the star parameters, we can use the following arguments. Near the overlap threshold, $R \cong D$, the concentration of counterions is almost uniform throughout the solution; i.e., $Q^*/Q \leq (1 - (R/D)^3)$. Under these conditions, the second, osmotic, term in the right-hand side of eq 9 predominates over the other terms. Expanding the right-hand side of eq 8 in powers of $(1 - (R/D)^3)$ and substituting the result in eq 9, we obtain (neglecting the excluded-volume interactions)

$$D^* \cong R^* \cong (l_B N^3)^{1/4} \Delta^{1/4} (f/m^2)^{1/4} \qquad (21)$$

We expect that the above equation is valid in a wide range of f, including $f \geq f^*$, provided Δ is larger than the intrinsic screening length near the edge of the star. In Figure 15, calculated values of D^* are plotted vs f/m^2 on a double-logarithmic scale. The observed dependence is close to the linear one that is expected from the scaling arguments presented above. The slope is smaller than expected from eq 21 under the assumption of Gaussian fluctuations of the extension of branches; i.e., $\Delta \sim N^{1/2}$. This difference can be explained by nonnegligible contributions of other interaction terms in eq 9.

Comparing eq 21 to eqs 15, 16, we find that the ratio R_{dilute}/D^* is expected to vary nonmonotonically with increases in f, i.e. a weak increase for small $f \leq f^*$ and a decrease for large f. This conclusion is in qualitative agreement with Figure 14.

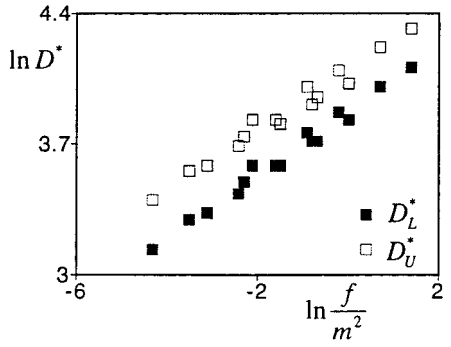

Figure 15. The parameter D^* as a function of f/m^2 for different f and m. The open symbols refer to D^*_U and the closed symbols to D^*_L.

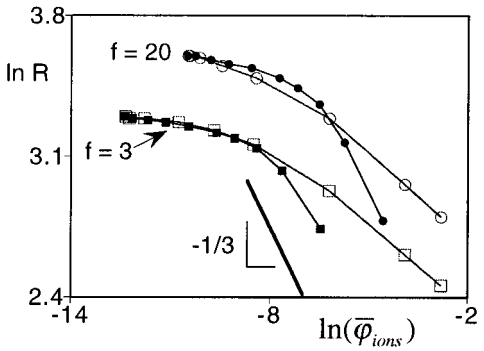

Figure 16. Star size R as a function of the average volume fraction of mobile ions $\bar{\varphi}_{ions}$ in the cell (in double-log coordinates) for $f = 3$ and 20 (Θ solvent, $N = 100$, $m = 5$). The open symbols refer to the case where the salt concentration is varied and $D = const = 200$. The closed symbols correspond to the calculations where $\varphi_s^b = const = 10^{-7}$ and D is varied.

It is instructive to compare the conformational changes in the star induced by an increase of the salt concentration (at small and constant concentration of polyelectrolytes in the solution) or by an increase of the polyelectrolyte concentration at low and constant concentration of salt. In the latter case, the screening of intramolecular Coulombic repulsion is provided by counterions, while in the former case, both co-ions and counterions contribute to screening. In Figure 16, the star size is plotted as a function of the average volume fraction of the mobile ions $\bar{\varphi}_{ions}$ in the cell. Open points correspond to a salt-induced deswelling of the star, whereas closed points show the decrease in the star size with decreasing cell size (equivalent to the increase in the concentration of stars in the solution). The "initial" points of both curves correspond to the star in the cell of radius $D = 200$ and with the bulk value of the salt concentration $\varphi_s^b = 10^{-7}$ and, obviously, coincide.

At high salt concentration, the star size R decreases as $R \sim (\varphi_s^b)^{-1/5}$, which corresponds to the linear the part of the curve describing screening by salt; the slope is close to the predicted value of $-1/5$. For the salt-free case, large values of $\bar{\varphi}_{ions}$ correspond to a small cell size D when geometrical confinement of the star in a cell occurs, $D < D^*$. Therefore, the ln R vs ln $\bar{\varphi}_{ions}$ curve tends to become linear with a slope $-1/3$,[33] thus going below the curve of screening by added salt.

The relative strength of intrastar screening (manifested in the star size) due to added salt or due to increased polyelectrolyte concentration in the intermediate range depends on the degree of branching.

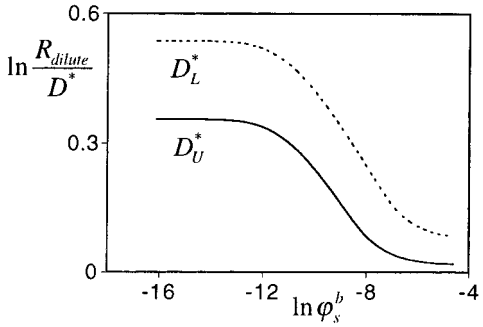

Figure 17. Relative magnitude of the maximal star contraction in the dilute regime, R_{dilute}/D^*, as a function of the volume fraction of salt in the bulk φ_s^b (in double-log scale). The solid curve corresponds to D^*_U and the dotted curve to D^*_L (Θ-solvent conditions, $N = 200$, $m = 5$, $f = 20$).

For $f = 3$, the distribution of counterions between inter- and intrastar space is in a salt-free case almost uniform even in dilute solution (see Figure 7) and becomes more uniform with increasing concentration of the solution. As a result, the enhanced screening effect of polyelectrolyte concentration appears to be almost the same as that of the salt concentration in a wide range of concentrations below c^* (corresponding to the overlap of the stars in a salt-free solution).

The situation is different in the solution of many-armed stars, $f = 20$, where the distribution of counterions (in the absence of salt) at small concentrations of polyelectrolytes is strongly nonuniform (see again Figure 7). At concentrations far below the overlap threshold c^*, a decrease of interstar distance (decrease in D) does not significantly affect the intrastar screening and star conformation because intrastar space contains only a small fraction of all counterions. As a result, the star remains more swollen than in the salt-added solution with the same average concentration of mobile ions. The star size starts to decrease rapidly (as $R \sim c^{-1/3}$) as the overlap threshold is approached, and the confinement of the stars comes into play. This behavior is consistent with an earlier scaling prediction[13] for the many-armed polyelectrolyte stars. We remark that, for many-armed stars, the regime of close packing without considerable interpenetration is expected to occur in a wide range of concentrations above the overlap threshold, $c > c^*$, i.e. in a semidilute solution. Therefore we expect that our cell model provides a correct description of the crossover between dilute and semidilute regimes, although it loses its applicability above the overlap threshold c^*.

The concentration effects in the regime of dilute solution become less pronounced as salt is added to the solution of star polyelectrolytes. The salt concentration imposes the bulk screening length, $\kappa_s^{-1} \cong l_B(\varphi_s^b)^{-1/2}$. We expect that the concentration effects are negligible unless the interstar distance, D, is smaller than κ_s^{-1}. On the other hand, the intramolecular screening turns out to be dominated by salt when the bulk screening length κ_s^{-1} becomes smaller than the intrinsic screening length κ_i^{-1}, which, for many-armed stars, is much smaller than the overall star size R.

In Figures 17 and 18, we give some additional information on the behavior of D^* as a function of the bulk volume fraction of salt φ_s^b. Figure 17 shows that, for high salt concentration, D^* becomes close to R_{dilute}. In this regime, the charge is almost completely screened and the polyelectrolyte star behaves like a neutral one.

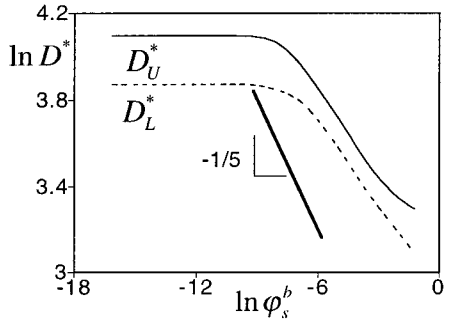

Figure 18. Parameter D^* as a function of the volume fraction of salt in the bulk φ_s^b (in double-log scale). The solid curve corresponds to D_U^* and the dotted curve to D_L^* (Θ solvent, $N = 200$, $m = 5$, $f = 20$).

In Figure 18, it is shown that D^* depends in the same way as R on φ_s^b, see also eq 19.

6. Discussion and Conclusions

On the basis of the numerical SCF approach, we have analyzed the conformational structure of star-branched polyelectrolytes in dilute solution. The effect of the degree of branching and the salt and polyelectrolyte concentrations on the screening of intramolecular Coulombic repulsion was studied systematically. The SCF results confirm the general trends predicted earlier on the basis of a scaling approach and provide better insight into the behavior in the crossover regions, where non-power dependencies of large-scale and local conformational properties on the molecular and solution parameters play an important role.

It is shown that, in dilute salt-free solutions, the distribution of counterions is strongly inhomogeneous: their local concentration is much higher in the intrastar space and rapidly decreases in the bulk of the solution. The effect of localization of the counterions in the intrastar space becomes stronger with an increasing number of branches f in the star. As a result, the intramolecular Coulombic repulsion in many-armed stars is strongly screened. This is manifested in a leveling off of the f dependence on the star size at large f.

We remark that the mean-field approach used in the present paper does not allow us to take into account the fluctuation-induced attractive electrostatic forces between the star branches. These forces arise due to strong local fluctuations of the concentration of counterions near strongly charged polyions and become important at sufficiently large values of the Bjerrum length. One can expect that this effect is stronger for highly branched polyions in comparison to that for linear ones because of the larger concentration of counterions in the intrastar space. However, the analysis of this phenomenon goes beyond the Poisson−Boltzmann approximation used in the present paper.

With increasing concentration of polyelectrolytes, the decrease in the translational entropy of counterions results in their progressive redistribution from the bulk of the solution to the intrastar space and in additional screening of the Coulombic repulsion between charged monomers. Therefore, the star size decreases. Significant star contraction is observed with increasing concentration of polyelectrolytes in the regime of dilute solution, i.e. below the overlap threshold for branched polyions. The effect is less pronounced in a solution of many-armed stars, which retain most of the counterions in the intrastar space, even in the dilute regime. In this case, an increase in the average solution concentration does not affect the local (intramolecular) counterion concentration, and as a result, the intramolecular screening is not changed. Hence, screening of intramolecular Coulombic repulsion is determined not only by the average solution concentration but also strongly by the molecular architecture.

We have analyzed the structural changes in the polyelectrolyte star induced by increasing the concentration of the solution and have identified the crossover concentration c^*. This concentration corresponds to close packing of stars which are already partially deswollen in the dilute regime due to enhanced intramolecular screening. At concentrations above c^*, our cell model describes the geometrical confinement of the star. If this model is mapped to a (star) polyelectrolyte solution, then c^* corresponds to the crossover to the semidilute regime. With increasing concentration above c^*, overlapping and partial interpenetration of the stars in solution occur. However, in analogy to semidilute solutions of neutral stars, we expect that, for many-armed stars, there is a wide concentration range where star contraction occurs with increasing concentration according to the power law $R \sim c^{-1/3}$, i.e. without significant interpenetration. The reason is, obviously, the remaining extension of the star branches with respect to the dimension of an individual polymer chain in the semidilute solution of the same concentration. Only at concentrations considerably above the overlap threshold, $c \gg c^*$, does such interpenetration become significant, and the structure of the solution becomes the same as that of the solution of individual linear chains of length N.

Our analysis of the effect of added salt on the polyelectrolyte star conformation in the dilute regime shows that the star size is virtually independent of the salt concentration over a wide range because of intrinsic screening by counterions. The onset of salt-induced star contraction corresponding to a crossover to the dominance of salt in the intramolecular screening is shifted to higher salt concentration as the number of branches in the star increases. This prediction is in a good agreement with experimental results[34] demonstrating low sensitivity of polyelectrolyte stars to added salt in comparison to their linear analogues. In the salt-dominance regime, the star size decreases as $R \sim (\varphi_s^b)^{-1/5}$ according to earlier scaling predictions.[14]

The comparison of the effect of added salt and that of increasing polyelectrolyte concentration on the star conformation shows that, in the dilute regime, the star size is less sensitive to increase of polyelectrolyte concentration than to addition of salt. This effect is due to the strongly inhomogeneous distribution of counterions in a salt-free dilute solution of many-armed stars. The difference between the two mechanisms of screening becomes less significant as the number of arms in the stars decreases: for stars with small numbers of branches, it is the average concentration of mobile ions that determines intramolecular screening.

Acknowledgment. O.V.B. is grateful to M. Daoud for many inspiring discussions and appreciates the hospitality of Prof. G. Fleer and Prof. M. Cohen Stuart at the University of Wageningen. E.B.Z. acknowledges the hospitality of Prof. A. C. Balazs at the University

of Pittsburgh. This work was partially supported by the NWO Dutch-Russian Program for Agricultural and Food Research and RFBR Grant 96-15-97401.

References and Notes

(1) Oosawa, F. *Polyelectrolytes*; Dekker: New York, 1971.
(2) Barrat, J.-L.; Joanny, J.-F. In *Advances in Chemical Physics*; Prigogine, I., Rice, S. A., Eds.; John Wiley: New York, 1996; Vol. 94.
(3) Napper, D. H. *Polymeric Stabilization of Colloidal Dispersions*; Academic Press: London, 1985.
(4) Marko, J. F.; Rabin, Y. *Macromolecules* **1992**, *25*, 1503.
(5) Wittmer, J.; Joanny, J.-F. *Macromolecules* **1993**, *26*, 2691.
(6) Guenoun, P.; Lipsky, S.; Mays, J. W.; Tirrel, M. *Langmuir* **1996**, *12*, 1425. Guenoun, P.; Davis, H. T.; Tirrel, M.; Mays, J. W. *Macromolecules* **1996**, *29*, 3965. Guenoun, P.; Delsanti, U.; Gazeau, D.; Mays, J. W.; Cook, D. C.; Tirrel, M.; Auvray, L. *Eur. Phys. J. B* **1998**, *1*, 77.
(7) Manning, G. *J. Chem. Phys.* **1969**, *51*, 924, 934, 3249.
(8) Pfeuty, P. *J. Phys. Fr.* **1978**, *39*, C2−149.
(9) Khokhlov, A. R.; Khachaturian, K. A. *Polymer* **1982**, *23*, 1742.
(10) Dobrynin, A. V.; Colby, R. H.; Rubinstein, M. *Macromolecules* **1995**, *28*, 1859.
(11) Daoud, M. *Self Similarity in Polyelectrolyte Solutions*; preprint.
(12) Stevens, M. J.; Kremer, K. *Phys. Rev. Lett.* **1993**, *71*, 2228. *Macromolecules* **1993**, *26*, 4717; *J. Chem. Phys.* **1995**, *103*, 1669.
(13) Borisov, O. V. *J. Phys. II* **1996**, *6*, 1.
(14) Borisov, O. V.; Zhulina, E. B. *Eur. Phys. J. B* **1998**, *4*, 205.
(15) Borisov, O. V.; Daoud, M. In preparation.
(16) Ziman, J. M. *Models of Disorder*; Cambridge University Press: Cambridge, U.K., 1979.
(17) The Coulombic contribution to the free energy of the cell can be obtained as $F_{\text{Coulombic}} = (\epsilon/2)\int_0^D (d\psi(r)/dr) r^{22}\, dr$ where the strength of the electrostatic field is given by $-d\psi(r)/dr = (4\pi/\epsilon r)^2 \int_0^r r' q^2(r')\, dr'$ and the local charge density (in the frame of our uniform approximation) is equal to $q(r) = 3Q^*/4\pi R^3$ at $r \le R$ and $q(r) = -3Q^*/4\pi(D^3 - R^3)$ at $R \le r \le D$, respectively.
(18) Daoud, M.; Cotton, J. P. *J. Phys. Fr.* **1982**, *43*, 531.
(19) Zhulina, E. B. *Polym. Sci. USSR* **1984**, *26*, 794.
(20) Birshtein, T. M.; Zhulina, E. B. *Polymer* **1984**, *25*, 1453. Birshtein, T. M.; Zhulina, E. B.; Borisov, O. V. *Polymer* **1986**, *27*, 1078.
(21) Kramarenko, E. Yu.; Khokhlov, A. R.; Yoshikawa, K. *Macromolecules* **1997**, *30*, 3383.
(22) Scheutjens, J. M. H. M.; Fleer, G. J. *J. Phys. Chem.* **1979**, *83*, 1619.
(23) Fleer, G. J.; Cohen Stuart, M. A.; Scheutjens, J. M. H. M.; Cosgrove, T.; Vincent, B. *Polymers at Interfaces*; Chapman & Hall: London, 1993.
(24) Israels, R.; Leermakers, F. A. M.; Fleer, G. J. *Macromolecules* **1994**, *27*, 3082.
(25) Alexander, S.; Chaikin, P. M.; Grant, P.; Morales, G. J.; Pincus, P.; Hone, D. *J. Chem. Phys.* **1984**, *80*, 5776.
(26) Pincus, P. *Macromolecules* **1991**, *24*, 2912. Ross, R.; Pincus, P. *Macromolecules* **1992**, *25*, 1503.
(27) The second virial coefficient of two elementary charged monomers interacting via DH potential $u_{\text{DH}}(r)/k_BT = l_B \exp(-\kappa r)/r$ is proportional to $\int(1 - \exp(-u_{\text{DH}}(r)/k_BT))r^2\, dr$. The latter integral is dominated by large r that results in eq 18.
(28) The normalized to one branch end segment distribution has been calculated as $\varphi_e(z) = L(z)\, \varphi(z|N)/f$.
(29) Zhulina, E. B.; Borisov, O. V.; Birshtein, T. M. *J. Phys. II* **1992**, *2*, 6. Zhulina, E. B.; Borisov, O. V. *J. Chem. Phys.* **1997**, *107*, 5952.
(30) Wijmans, C. M.; Zhulina, E. B. *Macromolecules* **1993**, *26*, 7214.
(31) The exponent $-4/3$ for the density profile directly follows from the exponent $3/5$ for the molecular weight dependence of the overall star size; see eq 20.
(32) de Gennes, P.-G. *Scaling Concepts in Polymer Physics*; Cornell University Press: Ithaca, NY, 1979.
(33) The slope $-1/3$ follows directly from the condition that $\bar{\varphi}_{\text{ions}} \sim D^{-3}$ and in the confinement regime $R \sim D$.
(34) Mays, J. W. *Polym. Commun.* **1990**, *31*, 170.

MA981501W